Surface Iodide Defects Control the Kinetics of the CsPbI 3 Perovskite Phase Transformation

Zachery Wylie, Mirella Al Katrib, Rory Campagna, Jonathan Outen, Samuel Smith, Peter Ruffolo, Baptiste Bérenguier, Muriel Bouttemy, Philip Schulz, Jeffrey Christians

ACS Energy LETTERS

http://pubs.acs.org/journal/aelccp

LETTER

Surface Iodide Defects Control the Kinetics of the $CsPbI_3$ Perovskite Phase Transformation

Zachery R. Wylie, Mirella Al Katrib, Rory Campagna, Jonathan E. Outen, Samuel Smith, Peter Ruffolo, Baptiste Bérenguier, Muriel Bouttemy, Philip Schulz, and Jeffrey A. Christians*

Cite This: *ACS Energy Lett.* 2024, 9, 4378−4385

Read Online

ACCESS | Metrics & More | Article Recommendations | Supporting Information

ABSTRACT: **Halide perovskites are technologically interesting across a wide range of optoelectronic devices, especially photovoltaics, but material stability has proven to be challenging. One degradation mode of note is the meta stability of the perovskite phase of some material compositions. This was studied by tracking the change of $CsPbI_3$ from its optoelectronically relevant perovskite phase to its thermodynamically stable nonperovskite phase, δ-$CsPbI_3$. We explore kinetics as a function of surface chemistry and observe a quantitatively similar, ∼5-fold, reduction in the phase transition rate between neat films and those treated with CsI and CdI_2. Using XPS to explore surface chemistry changes across samples, we link the reduction in the phase transition rate to the surface iodide concentration. When informed by previous theoretical studies, these experiments point to surface iodide vacancies as the nucleation sites for δ-$CsPbI_3$ growth and show that phase nucleation is the rate limiting step in δ-$CsPbI_3$ formation for $CsPbI_3$ perovskite thin films.**

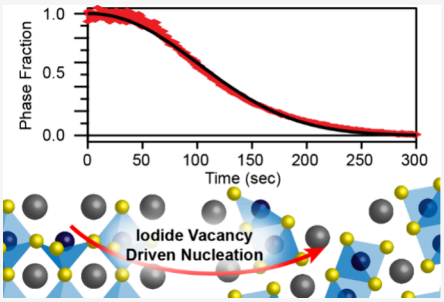

Metal halide perovskites will likely grow to be disruptive materials in the world of optoelectronics. Their exceptional charge carrier mobilities,[1] and high photoluminescent quantum yields (PLQY),[2] make for solar cells with efficiencies as high as 26.1%.[3,4] Coupled with low processing costs,[5] and the possibility for their integration into tandem architectures,[6] these solar cells promise to be transformative in the energy sector. $CsPbX_3$ (X = Cl, Br, I) are the most widely studied class of all-inorganic halide perovskites due to a high thermal stability and suitable bandgap for photovoltaic applications.[7] $CsPbX_3$ exhibits three perovskite phases: cubic (α, *Pm*3*m*), tetragonal (β, *P*4/*mbm*), and orthorhombic (γ, *Pbnm*). At room temperature, it is common for $CsPbI_3$ to relax locally into the orthorhombic perovskite phase.[8,9] There also exists a nonperovskite, orthorhombic phase (δ, *Pnma*) that does not strongly absorb solar irradiation due to a wide band gap and has poor charge transport.[10] Unfortunately, at room temperature the δ-phase is thermodynamically favored.[11] It is known that moisture catalyzes the transition from the metastable γ-$CsPbI_3$ into δ-$CsPbI_3$. Also, because of ion mobility, δ-$CsPbI_3$ can form in mixed cation formulations such as $FA_xCs_{1-x}PbI_3$ (FA = formamidinium).[12] Therefore, while this class of inorganic halide perovskites is promising, the phase transition to the nonperovskite δ-phase remains the most significant hurdle to commercial implementation.[5]

Such phase transitions are important beyond just $CsPbI_3$. In the hybrid organic inorganic lead halide perovskite methylammonium lead iodide ($MAPbI_3$), moisture intercalates into the crystal lattice, forming metal hydrates, disrupting the structure.[13,14] More similarly, a perovskite to nonperovskite phase transition plagues formamidinium lead iodide ($FAPbI_3$) and FA-based alloys,[12,15,16] the materials that form the backbone of most of the highest performing devices,[17] although $FAPbI_3$ transforms into different nonperovskite phases.[18] Molecular dynamic simulations suggest that surface moisture amplifies surface halide vacancies by strongly solvating halide ions at the interface.[19] This is also seen in the moisture-assisted self-healing of halide perovskite films.[20] Vacancies such as these locally deform the structure resulting in octahedral tilting into the nonperovskite phase.[21,22] This previous evidence suggests that the moisture-induced phase transition of inorganic lead halide perovskites is, at its core, a function of surface halide vacancies and ion mobility more than it is a consequence of water adsorption. In this study, we build on previous experimental and theoretical work,[22−27] to provide a more conclusive experimental picture of the role that surface halide vacancies play in the appearance of δ-$CsPbI_3$ in perovskite thin films.

Received: May 30, 2024
Revised: August 1, 2024
Accepted: August 12, 2024
Published: August 15, 2024

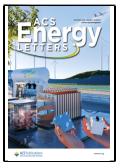

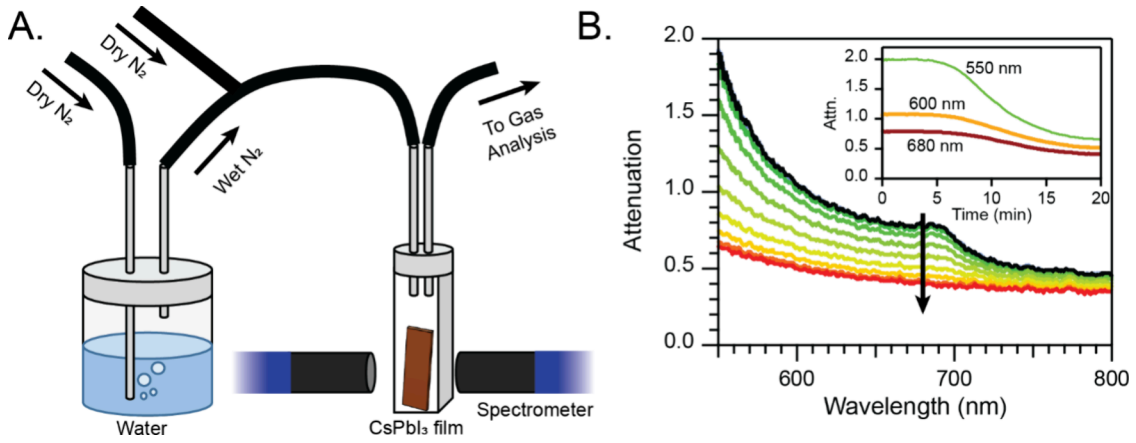

Figure 1. A) Diagram of the atmosphere-controlled absorption spectrometer system used for many of these experiments, and B) representative traces taken with this system as a $CsPbI_3$ perovskite film undergoes a phase transition to the nonperovskite δ-phase. The inset shows kinetic traces extracted at several different wavelengths from this data.

Surface treatment has proven to be an effective strategy for improving the moisture resistance of perovskites,[28,29] whether using hydrophobic surface ligands such as oleylamine to limit water adsorption and passivate defects,[30] or filling specific vacancies by treating a film with coordinating organic ligands.[31−33] Very recently, Guo et al. performed a comprehensive theoretical investigation into the structural collapse of $CsPbI_3$.[22] From their calculations, they concluded that kinetic, rather than thermodynamic, aspects dominate the phase stability of $CsPbI_3$ and that iodide vacancies provide the nucleation sites. In this work, we aim to improve the experimental evidence for or against an iodide vacancy driven mechanism and to experimentally reveal the rate limiting step in δ-$CsPbI_3$ formation. To differentiate between X-site vacancies and other effects, we passivated these vacancies using both CdI_2 and CsI treatments. We use the Johnson−Mehl−Avrami−Kolmogorov (JMAK) model to describe the transformation and extract kinetic information on surface treatments with respect to increasing both CdI_2 and CsI concentrations, showing that each of these treatments slows the phase transformation by a similar factor of ∼5. The analogous behavior of the two treatments, in terms of both the increase in surface iodide concentration and the slowed transition, points toward iodide vacancy filling, rather than Cs- or Pb-vacancies, as the dominant mechanism slowing the δ-phase transition. Microscopy further supports nucleation as the rate limiting step of the phase change.

In this report, $CsPbI_3$ thin films spin coated on FTO glass substrates are used as a representative system to track the phase transformation. Two distinct film preparation methods were used, one with a methyl acetate antisolvent,[34] and one with a simple one-step from DMF with no antisolvent.[35] After annealing, as-synthesized $CsPbI_3$ films were treated with a CdI_2 or CsI solution in IPA. To control the exposure of the films to constant humidity and temperature, an ad hoc flow apparatus was built (Figure 1A), which allowed for fine control over the environment (Figure S1) by bubbling nitrogen through deionized water. It should be noted that the humid air flow in the system led to increased rates due to decreased boundary layer thickness but yielded similar data to those of $CsPbI_3$ films in still air (Figure S2). The temperature of the substrate was measured directly with a thermocouple. In this way, the nitrogen flow rate determined the %RH, which allowed for a high degree of control over the kinetics of the perovskite phase transition.

The direct transmittance through the perovskite film was measured, and the attenuation (absorbance plus scattering/reflection) at 680 nm was used to track the phase transition over time since the black perovskite phase is easily distinguishable from the yellow nonperovskite phase at this wavelength. Figure 1B shows this phase transition as a series of attenuation measurements taken over 20 min with the black curve showing the perovskite phase at the start and the red trace showing the nonperovskite δ-phase. This spectroscopic data was then used to determine the phase fraction of the γ-$CsPbI_3$ perovskite. To do this, we assume the 100% perovskite phase initially at the maximum attenuation (μ_{100}) and the 100% nonperovskite phase at the minimum attenuation (μ_0) and relate these linearly to the $CsPbI_3$ perovskite phase fraction, $x = (\mu - \mu_0)/(\mu_{100} - \mu_0)$. A typical phase transition of a $CsPbI_3$ film treated only with IPA occurred over approximately 5 min at 20%RH and 20 ± 1 °C in our flow apparatus. For a clear attribution of these observed changes in the optical properties to a crystallographic phase change, we require a direct experimental probe of the structural properties. We thus confirmed by powder X-ray diffraction (XRD) measurements that the initial and final films are in fact 100% perovskite and nonperovskite phase, respectively (Figure S3). Importantly, the dynamics of the phase transition are the same as when measuring the powder XRD pattern (Figure S4) as with UV−vis spectroscopy, and the diffraction data show a quantitative agreement between the disappearance of $CsPbI_3$ perovskite and the growth of δ-$CsPbI_3$. The JMAK model, which is widely used to describe phase transitions in bulk and thin film systems,[36−41] takes the following form,

$$x = e^{-(kt)^n} \tag{1}$$

where k is the effective rate constant, and n is the Avrami constant, or shape factor. Both n and k consist of contributions from phase nucleation and phase growth through multiple dimensions.[42] A natural log plot of time and the natural log of the phase fraction extract the shape factor n as the slope of the resulting straight line as well as the natural log of the effective rate constant k at its intercept.

$$\ln(-\ln(x)) = n\ln(t) + \ln(k) \tag{2}$$

https://doi.org/10.1021/acsenergylett.4c01465
ACS Energy Lett. 2024, 9, 4378−4385

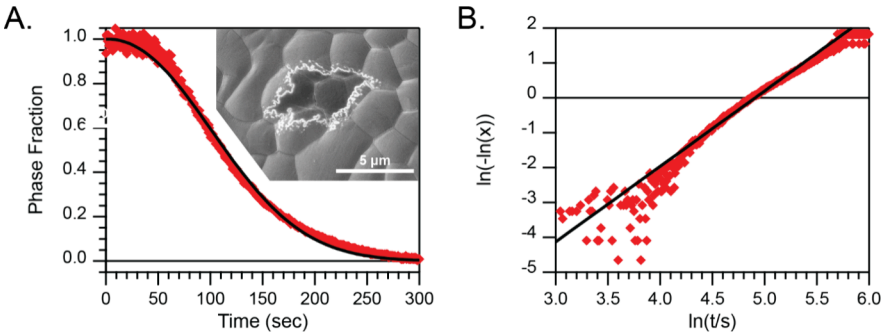

Figure 2. A) Transformed UV−visible spectroscopy kinetic data into phase fraction, *x*, of the $CsPbI_3$ perovskite phase for a representative $CsPbI_3$ thin film, fit by eq 1 (black line). The inset shows an SEM image of a central δ-$CsPbI_3$ region surrounded by γ-$CsPbI_3$. B) The transformation of (A) by eq 2 has a linear slope of the growth shape factor "*n*".

The JMAK model is valid for particle growth and phase transitions assuming that (i) the system is infinitely large in comparison to the size of the germinating phase, (ii) the nucleation is homogeneous throughout the material, (iii) the growth of the phase terminates when it impinges on growth from other nucleation sites, and (iv) the process is isothermal.[43−45] The phase transition of a black $CsPbI_3$ perovskite film to the yellow nonperovskite δ-phase is well described by JMAK kinetics (Figure 2 and Figure S4). However, the geometry of the system requires a more careful consideration. In thin film systems where it is possible that the size of the phase germ is no longer negligible compared to the thickness of the film, or when phase nucleation occurs at an interface, the shape factor is predicted to become nonconstant toward the end of the phase transformation when the germinated cells impinge upon an interface.[46,47] This, however, should only be noticeable when the thickness of the film reaches an appreciable size when compared to the phase nucleation density.[48] In the present experiments, film thickness is approximately 500 ± 100 nm (Figure S5) and is significantly smaller than the diameter of most nonperovskite domains in partially transformed films (Figure S6). However, in some experiments, a slight change in the shape factor is seen near the end of the experiments (shown in Figure 2B by the slight change in the slope as well as in some other experiments). With this in mind, the JMAK equation is appropriate for modeling $CsPbI_3$ kinetics between samples if films are kept at consistent thicknesses and the temperature is constant.

Looking more closely at the representative data in Figure 2, noise is responsible for the deviation from the eq 2 model when $\ln(-\ln(x)) \geq -2$ due to the asymptotic nature of the *y*-axis. The shape factor, *n*, was found to be 2.14 ± 0.29 across 10 different treated and untreated $CsPbI_3$ thin films (Table S1, Figure 3). If we assume that the majority of the phase transition occurs within a 2D regime, the shape factor is expected to be 2 if nucleation of the δ-phase is homogeneous and 3 if nucleation is heterogeneous.[42,49] Looking at SEM images of partially transformed films (see inset, Figure 2A and Figure S6), we see that the growth of the nonperovskite δ-phase is often anisotropic. Anisotropic growth would tend to reduce the shape factor. Taken together, the observed shape factor suggests that the phase transformation appears to be a mix of homogeneous and heterogeneous nucleation (from surface adsorbed water) and occurs primarily in the 2D regime. Overall, the phase transition is nucleation rate limited rather than limited by the growth rate, as clearly seen by the sparse, large crystallites in partially transformed films (Figure S6). This

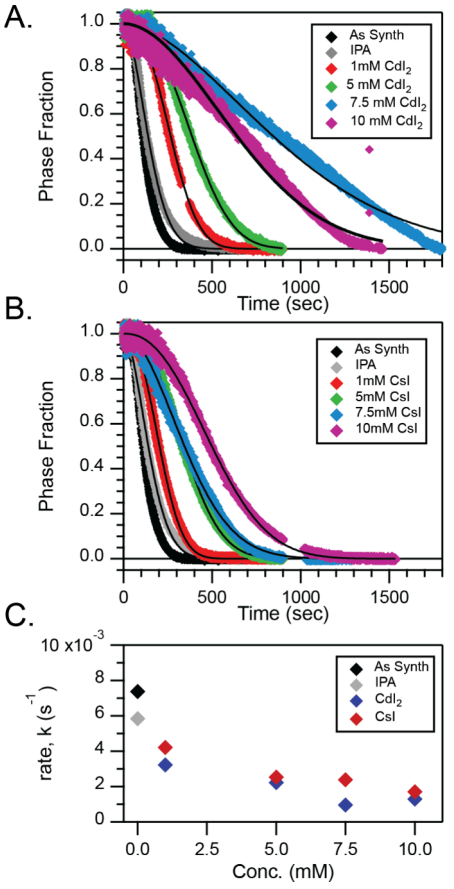

Figure 3. Kinetics of phase change (from UV−visible spectroscopic data) for $CsPbI_3$ thin films treated with varying concentrations of (A) CdI_2, and (B) CsI in IPA. C) The rate constant extracted from the JMAK fits (solid black lines) shows a quantitatively similar change in phase change kinetics for both treatments.

is similar to experiments by Lin et al. that determined a difference in these two rates of ∼10−1000 in their experiments with $CsPbI_3$ microcrystals.[50]

While, in the present case, the contributions of phase nucleation and phase growth are convoluted; nevertheless, these results point to the immense importance of surface chemistry in the phase transformation rate. Therefore, we selected two different surface treatments, one with CsI and one with CdI_2, to explore their contributions to this rate. Both treatments were done following standard $CsPbI_3$ film formation by coating the film with a CsI or CdI_2 solution in

https://doi.org/10.1021/acsenergylett.4c01465
ACS Energy Lett. 2024, 9, 4378−4385

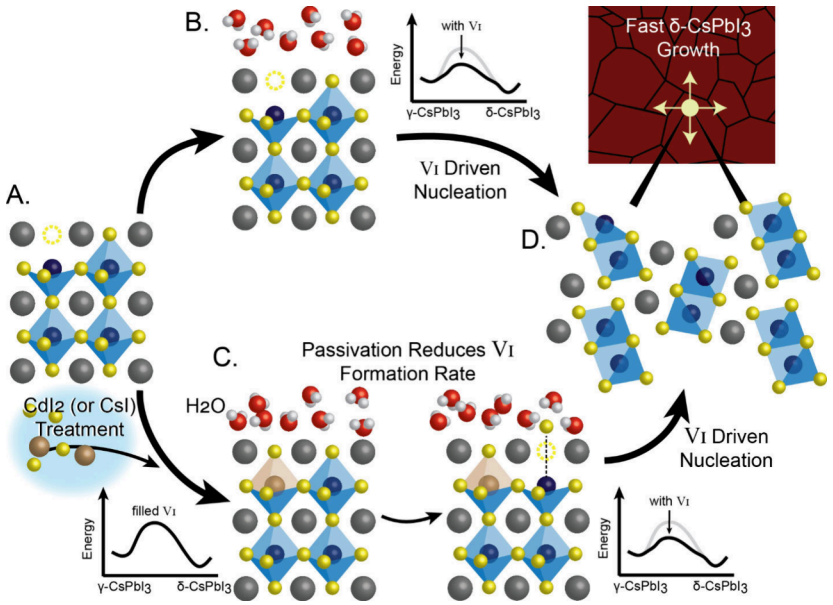

Figure 4. Schematic showing the proposed mechanism for the transformation from γ-$CsPbI_3$ perovskite phase to nonperovskite δ-$CsPbI_3$. A) As-synthesized $CsPbI_3$ film with surface iodide vacancies, B) rapidly forms δ-$CsPbI_3$ germs because of the reduced kinetic barrier for phase transformation caused by iodide vacancies. On the other hand, C) CdI_2 (and CsI) treatments fill iodide vacancies, and lead to a reduced rate of δ-$CsPbI_3$ germ nucleation. D) Once nucleated, the δ-$CsPbI_3$ phase spreads rapidly through the perovskite film.

IPA and annealing. These two salt treatments were selected to change the surface stoichiometry of the films to be richer in AX or BX_2 species and thus to elucidate how these surface chemistry changes relate to the phase change kinetics.

By relating the change in attenuation at 680 nm to the phase fraction as previously described, both CsI and CdI_2 treatments are shown to result in slower phase transition kinetics at constant temperature and humidity, despite the fact that these salts are both very soluble in water, which would make them a poor physical barrier for moisture.[51] Figure 3A,B shows plots of the phase fraction of the perovskite phase over time for different salt concentrations of CdI_2 and CsI treatments, respectively, in a constant environment. All phase transitions, regardless of treatment, have shape factors within the range of nontreated films, which suggests that the mechanism is consistent across as-synthesized and treated films. Control films treated with pure IPA showed an effective rate constant of 5.8×10^{-3} s^{-1} while films treated with CdI_2 (7.5 mM) and CsI (10 mM) showed this rate reduced approximately 5-fold to an effective rate constant of 9.6×10^{-4} s^{-1} and 1.7×10^{-3} s^{-1}, respectively. As these treatments do not lead to significant changes in the initial film morphology (Figure S7), we propose that the surface chemistry is the dominant cause of the rate reduction. When the charge carrier recombination kinetics were investigated by time-resolved photoluminescence (TRPL), the treated samples showed longer lifetimes (Figure S8), consistent with a surface passivation effect. To confirm that this treatment was not limited to one specific film fabrication method, we corroborated these findings with $CsPbI_3$ films made with a simple one-step process from DMF (Figure S9) as well as in multiple side-by-side trials done with films under uncontrolled ambient conditions.

Other treatments have also been found to successfully slow the $CsPbI_3$ δ-phase transition, but the specific mechanism has remained somewhat obfuscated. Following a recent theoretical investigation, however, Guo et al. described iodide vacancies as, "the seed of the whole phase transition process."[22] Our nearly identical effects observed with CsI and CdI_2 treatment also point to the common element, iodide, as the most likely cause behind the reduced phase transformation rate with less influence from the A- or B-site. Below, we propose a mechanism for the γ-$CsPbI_3$ to δ-$CsPbI_3$ phase transition based on our own observations, and informed by the literature (Figure 4). While there have been studies identifying control over transition rate through the relative stability of the γ- and δ-$CsPbI_3$ phases,[52,53] thermodynamics alone cannot account for the rate of the transition.[22] The phase transition has been shown via DFT by Chen et al. to be a multistep process dominated by kinetics that are accelerated by iodine vacancies (V_I) at the surface (Figure 4B–D) when water is introduced.[54] These vacancies lower the barrier to the first transition state by mediating the first intermediate state with additional short-lived states that are not present in the pristine lattice phase transition pathway.[22] Passivating V_I, which in this study is done via iodine salt treatment (Figure 4A–C), raises the overall kinetic barrier and reduces the rate of δ-$CsPbI_3$ nucleation. Once the δ-phase has nucleated, however, the growth proceeds rapidly in a domino effect.[55,56] This study corroborates the conclusion that the phase transition is slowed primarily by limiting nucleation of δ-$CsPbI_3$ as the shape factor from the JMAK model is similar for both the treated and untreated films, indicating that the growth mechanism is unaffected. To fully understand the effect that the CdI_2 and CsI treatments have on the surface of the films, it is important to provide a clearer picture of the surface chemistries in treated and untreated cases to correlate the change in kinetics with V_I passivation.

To accomplish this goal, X-ray photoelectron spectroscopy (XPS) measurements were performed on a range of samples, with measurements taken at two points on each sample. XPS allows for elemental quantification of the near-surface region, with the signal coming mostly from the top ~5 nm of the sample. Thus, even though the measurement is surface-sensitive, the compositional analysis extends over the surface

https://doi.org/10.1021/acsenergylett.4c01465
ACS Energy Lett. 2024, 9, 4378–4385

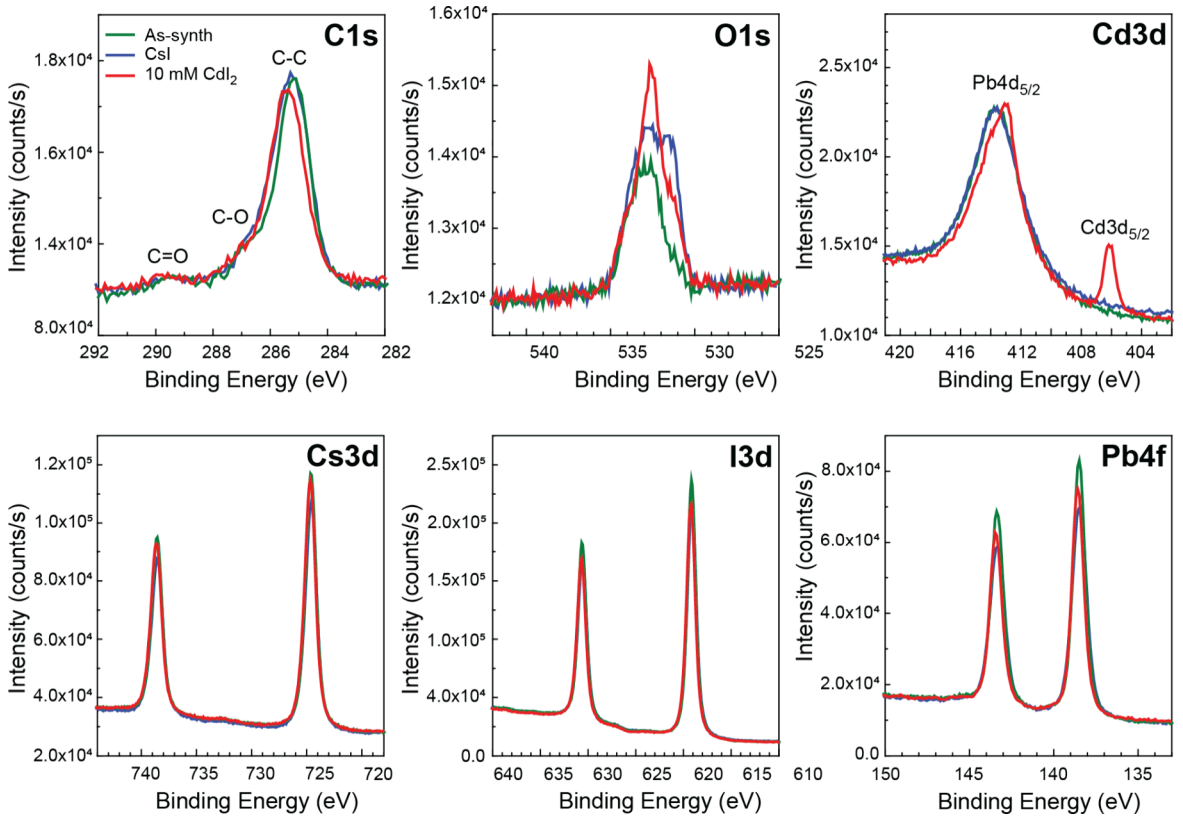

Figure 5. XPS measurements of the high energy resolution core levels spectra of C 1s, O 1s, Cd 3d, Cs 3d, I 3d, and Pb 4f for the untreated control film, the one treated with CsI and the one treated with CdI_2 (10 mM).

and the subsurface region of the probed sample. The samples included thin films of $CsPbI_3$ washed with pure IPA, $CsPbI_3$ treated with saturated CsI (~10 mM) in IPA, and 4 samples of $CsPbI_3$ treated with CdI_2 at concentrations in a range from 1 mM to 10 mM in IPA. Across all of the measured samples, no visible chemical shifts in the core level spectra or rise of additional peaks stemming from a different oxidation state were observed that would indicate a change in the chemical environment of the key elements that comprise the perovskite film (Cs, I, Pb), along with trace C and O contaminations. The high energy resolution spectra for the Cs 3d, I 3d, Pb 4f, Cd 3d, and O 1s orbitals were used to quantify the surface composition (Table S3). Of the 4 samples treated with increasing CdI_2, no specific trend was detected in surface composition of any chemical species meaning that the saturation of the surface chemical reaction is already reached for the lowest concentrations of CdI_2 (Figure S9, Table S4). Therefore, only results for the sample treated with 10 mM CdI_2 are presented in the main text from this sample set.

The high-resolution photopeaks of the detected elements for the samples treated with saturated CsI and 10 mM CdI_2 in IPA can be seen in Figure 5, with references to the as-synthesized control sample. The C 1s core level is positioned at 285.2 eV and presents a shape typical for adventitious carbon contamination with effectively constant C concentration across all samples. The O 1s core level indicates the presence of oxygen contamination possibly from residual IPA, or surface contamination, which is in agreement with the C−O and C=O contributions to the C 1s spectra at higher binding energies. In addition to C−O and C=O, another oxygen species was detected at a lower binding energy of 531 eV on the treated samples. This can be attributed to the formation of an oxidized metal such as PbO_X. However, due to the small chemical shift between Pb^{2+} and Pb^0, combined with the low oxide proportion, no widening of the Pb 4f peaks could be identified. The emergence of a Cd $3d_{5/2}$ peak at 406 eV also confirms the presence of Cd at the surface (less than 1 atomic%) when treating samples with CdI_2.

To investigate variations in the cation and halide surface concentrations, elemental ratios were calculated for the treated and untreated samples (Figure 6). Taking the elemental ratio

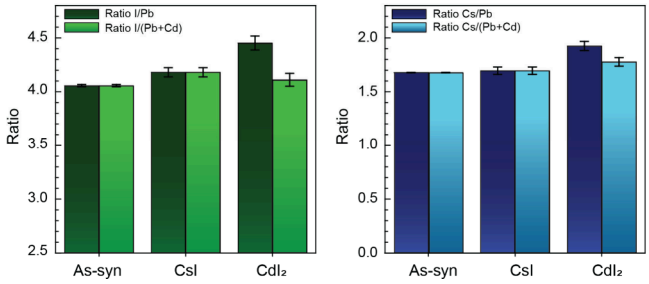

Figure 6. Comparison of key elemental ratios for the control film, the film treated with CsI, and the film treated with CdI_2 (10 mM).

helps to correct for differences in surface contamination (e.g., O and C signals) and provides a better basis for sample comparison. The I/Pb ratio shows a moderate increase when the films are treated with CsI, which confirms a rise in the surface concentration of iodide after the treatment. A more significant increase in the I/Pb ratio is seen for CdI_2 treated films; however, when the added Cd is taken into consideration for the CdI_2-treated sample by calculating the ratio I/(Pd

https://doi.org/10.1021/acsenergylett.4c01465
ACS Energy Lett. 2024, 9, 4378−4385

+Cd), we find that this new ratio is in line with the CsI treated films.[23] In contrast, the Cs/Pb ratio presents a negligible increase compared with the sample treated with CsI and a larger increase when treated with CdI_2. This seemingly perplexing observation that treating with CdI_2 increases the Cs^+ surface concentration more than a direct CsI treatment can be rationalized if Cd is filling Pb vacancies. In that case, we would expect that the CdI_2 treated films would have a Cs/(Pb +Cd) ratio, which is in line with the neat films. In this case, the Cs/(Pb+Cd) ratio is still slightly elevated when compared to the control films and the CsI treated films, but less extreme. Despite this evidence of Cd^{2+} substitution into the $CsPbI_3$ crystal, the dominant effect, from a phase stability standpoint, does appear to be the role that iodide vacancy filling plays between these two samples.

Controlling the phase transition from meta stable perovskite phases to nonperovskite δ-phases is critical to the stability of the majority of the halide perovskite materials that are, at present, more technologically interesting. In these experiments, we used $CsPbI_3$ perovskite as a model system to explore this phase transition in greater detail. The phase transition between the perovskite phase and the nonperovskite δ-phase was found to be well-described by the JMAK model of solid-state phase transitions. Surface treatments of the $CsPbI_3$ films with both CsI and CdI_2 show quantitatively similar results; both surface treatments slow the overall rate of the phase change by approximately a factor of 5. Using XPS, we were able to confirm that both treatments result in increased surface concentrations of iodide, presumably helping to passivate or slow the formation of iodide vacancies, while the CdI_2 treatment also appears to result in Cd^{2+} filling Pb^{2+} sites. These treatments did not change the phase transition mechanistically. More importantly, they functioned quantitatively similarly in slowing the phase transition process with similar increases in surface iodide concentrations despite differences in the concentrations of other surface species. Taken together with prior theoretical evidence, these experiments point strongly to iodide vacancies as the key nucleation sites for δ-phase formation in $CsPbI_3$ perovskites. Because of their high concentrations in $CsPbI_3$ thin films, we believe that the improved surface passivation of iodide vacancies will have a large kinetic effect on $CsPbI_3$ perovskite phase stability. These findings, hence, denote a step toward the targeted design of halide perovskite surfaces, which enables improved control of the perovskite to nonperovskite phase transition and thus eventually the improved reliability of halide perovskite-based optoelectronic devices.

■ ASSOCIATED CONTENT

Supporting Information

The Supporting Information is available free of charge at https://pubs.acs.org/doi/10.1021/acsenergylett.4c01465.

Experimental section, phase fraction plots, XRD spectra, SEM images, tables of kinetics parameters, tables of XPS compositions, XPS spectra (PDF)

■ AUTHOR INFORMATION

Corresponding Author

Jeffrey A. Christians − *Department of Engineering, Hope College, Holland, Michigan 49423, United States;* orcid.org/0000-0002-6792-9741; Email: christians@hope.edu

Authors

Zachery R. Wylie − *Department of Engineering, Hope College, Holland, Michigan 49423, United States; Department of Chemical Engineering, University of Washington, Seattle, Washington 98195, United States*

Mirella Al Katrib − *IPVF, Palaiseau 91120, France; Institut Lavoisier de Versailles (ILV), Versailles 78000, France*

Rory Campagna − *Department of Engineering, Hope College, Holland, Michigan 49423, United States*

Jonathan E. Outen − *Department of Engineering, Hope College, Holland, Michigan 49423, United States*

Samuel Smith − *Department of Engineering, Hope College, Holland, Michigan 49423, United States*

Peter Ruffolo − *Department of Engineering, Hope College, Holland, Michigan 49423, United States*

Baptiste Bérenguier − *IPVF, Palaiseau 91120, France; Institut Photovoltaïque d'Île-de-France (IPVF), Palaiseau 91120, France*

Muriel Bouttemy − *IPVF, Palaiseau 91120, France; Institut Lavoisier de Versailles (ILV), Versailles 78000, France*

Philip Schulz − *IPVF, Palaiseau 91120, France; Institut Photovoltaïque d'Île-de-France (IPVF), Palaiseau 91120, France;* orcid.org/0000-0002-8177-0108

Complete contact information is available at: https://pubs.acs.org/10.1021/acsenergylett.4c01465

Notes

The authors declare no competing financial interest.

■ ACKNOWLEDGMENTS

Research reported in this publication was supported by the National Science Foundation (DMR-2128632 and under Major Research Instrumentation Award No. 2117655). ZRW and PR acknowledge support by the National Aeronautics and Space Administration (NASA), under award number NNX15AJ20H, Michigan Space Grant Consortium (MSGC). Additional support was provided by the Howard R. And Margaret E. Sluyter Faculty Development Fund, and the Hope College Dean of Natural and Applied Sciences. JC acknowledges support by the Towsley Research Scholars Program grant from the Towsley Foundation of Midland, Michigan. This work was also supported by the French government in the framework of the program of investments for the future (Programme d"Investissement d'Avenir ANR-IEED-002-01).

■ REFERENCES

(1) Kang, Y.; Han, S. Intrinsic Carrier Mobility of Cesium Lead Halide Perovskites. *Phys. Rev. Applied* **2018**, *10* (4), 044013.

(2) Ahmad, W.; Khan, J.; Niu, G.; Tang, J. Inorganic $CsPbI_3$ Perovskite-Based Solar Cells: A Choice for a Tandem Device. *Sol. RRL* **2017**, *1* (7), 1700048.

(3) Zhang, J.; Hodes, G.; Jin, Z.; Liu, S. All-Inorganic $CsPbX_3$ Perovskite Solar Cells: Progress and Prospects. *Angew. Chem., Int. Ed.* **2019**, *58* (44), 15596−15618.

(4) *NREL Transforming Energy. Best Research-Cell Efficiency Chart.* https://www.nrel.gov/pv/cell-efficiency.html (accessed 2024-02-16).

(5) Faheem, M. B.; Khan, B.; Feng, C.; Farooq, M. U.; Raziq, F.; Xiao, Y.; Li, Y. All-Inorganic Perovskite Solar Cells: Energetics, Key Challenges, and Strategies toward Commercialization. *ACS Energy Lett.* **2020**, *5* (1), 290−320.

(6) Maxwell, A.; Chen, H.; Grater, L.; Li, C.; Teale, S.; Wang, J.; Zeng, L.; Wang, Z.; Park, S. M.; Vafaie, M.; Sidhik, S.; Metcalf, I. W.; Liu, Y.; Mohite, A. D.; Chen, B.; Sargent, E. H. All-Perovskite

Tandems Enabled by Surface Anchoring of Long-Chain Amphiphilic Ligands. *ACS Energy Lett.* **2024**, *9* (2), 520−527.
(7) Lin, J.; Lai, M.; Dou, L.; Kley, C. S.; Chen, H.; Peng, F.; Sun, J.; Lu, D.; Hawks, S. A.; Xie, C.; Cui, F.; Alivisatos, A. P.; Limmer, D. T.; Yang, P. Thermochromic Halide Perovskite Solar Cells. *Nat. Mater.* **2018**, *17* (3), 261−267.
(8) Hoffman, A. E. J.; Saha, R. A.; Borgmans, S.; Puech, P.; Braeckevelt, T.; Roeffaers, M. B. J.; Steele, J. A.; Hofkens, J.; Van Speybroeck, V. Understanding the Phase Transition Mechanism in the Lead Halide Perovskite CsPbBr3 via Theoretical and Experimental GIWAXS and Raman Spectroscopy. *APL Materials* **2023**, *11* (4), 041124.
(9) Schelhas, L. T.; Christians, J. A.; Berry, J. J.; Toney, M. F.; Tassone, C. J.; Luther, J. M.; Stone, K. H. Monitoring a Silent Phase Transition in $CH_3NH_3PbI_3$ Solar Cells via *Operando* X-Ray Diffraction. *ACS Energy Lett.* **2016**, *1* (5), 1007−1012.
(10) Tan, X.; Wang, S.; Zhang, Q.; Liu, H.; Li, W.; Zhu, L.; Chen, H. Stabilizing CsPbI3 Perovskite for Photovoltaic Applications. *Matter* **2023**, *6* (3), 691−727.
(11) Wang, Y.; Chen, Y.; Zhang, T.; Wang, X.; Zhao, Y. Chemically Stable Black Phase $CsPbI_3$ Inorganic Perovskites for High-Efficiency Photovoltaics. *Adv. Mater.* **2020**, *32* (45), 2001025.
(12) Schelhas, L. T.; Li, Z.; Christians, J. A.; Goyal, A.; Kairys, P.; Harvey, S. P.; Kim, D. H.; Stone, K. H.; Luther, J. M.; Zhu, K.; Stevanovic, V.; Berry, J. J. Insights into Operational Stability and Processing of Halide Perovskite Active Layers. *Energy Environ. Sci.* **2019**, *12* (4), 1341−1348.
(13) Yang, J.; Siempelkamp, B. D.; Liu, D.; Kelly, T. L. Investigation of $CH_3NH_3PbI_3$ Degradation Rates and Mechanisms in Controlled Humidity Environments Using *in Situ* Techniques. *ACS Nano* **2015**, *9* (2), 1955−1963.
(14) Christians, J. A.; Miranda Herrera, P. A.; Kamat, P. V. Transformation of the Excited State and Photovoltaic Efficiency of $CH_3NH_3PbI_3$ Perovskite upon Controlled Exposure to Humidified Air. *J. Am. Chem. Soc.* **2015**, *137* (4), 1530−1538.
(15) Hidalgo, J.; Kaiser, W.; An, Y.; Li, R.; Oh, Z.; Castro-Méndez, A.-F.; LaFollette, D. K.; Kim, S.; Lai, B.; Breternitz, J.; Schorr, S.; Perini, C. A. R.; Mosconi, E.; De Angelis, F.; Correa-Baena, J.-P. Synergistic Role of Water and Oxygen Leads to Degradation in Formamidinium-Based Halide Perovskites. *J. Am. Chem. Soc.* **2023**, *145* (45), 24549−24557.
(16) Yun, J. S.; Kim, J.; Young, T.; Patterson, R. J.; Kim, D.; Seidel, J.; Lim, S.; Green, M. A.; Huang, S.; Ho-Baillie, A. Humidity-Induced Degradation via Grain Boundaries of $HC(NH_2)_2PbI_3$ Planar Perovskite Solar Cells. *Adv. Funct. Mater.* **2018**, *28* (11), 1705363.
(17) Liu, Z.; Liu, P.; Li, M.; He, T.; Liu, T.; Yu, L.; Yuan, M. Efficient and Stable FA-Rich Perovskite Photovoltaics: From Material Properties to Device Optimization. *Adv. Energy Mater.* **2022**, *12* (18), 2200111.
(18) Lai, M.; Lei, T.; Zhang, Y.; Jin, J.; Steele, J. A.; Yang, P. Phase Transition Dynamics in One-Dimensional Halide Perovskite Crystals. *MRS Bull.* **2021**, *46* (4), 310−316.
(19) Steele, J. A.; Lai, M.; Zhang, Y.; Lin, Z.; Hofkens, J.; Roeffaers, M. B. J.; Yang, P. Phase Transitions and Anion Exchange in All-Inorganic Halide Perovskites. *Acc. Mater. Res.* **2020**, *1* (1), 3−15.
(20) Parida, S.; Kumar, S.; Cherf, S.; Aharon, S.; Cahen, D.; Eren, B. Self-Healing and -Repair of Nanomechanical Damages in Lead Halide Perovskites. *Adv. Funct Materials* **2023**, *33* (45), 2304278.
(21) Ma, J.-P.; Yin, J.; Chen, Y.-M.; Zhao, Q.; Zhou, Y.; Li, H.; Kuroiwa, Y.; Moriyoshi, C.; Li, Z.-Y.; Bakr, O. M.; Mohammed, O. F.; Sun, H.-T. Defect-Triggered Phase Transition in Cesium Lead Halide Perovskite Nanocrystals. *ACS Materials Lett.* **2019**, *1* (1), 185−191.
(22) Guo, Z.; Fu, J.; Chen, G.; Liu, F.; Yu, C.; Lu, R.; Yin, W. First Domino in the Structural Collapse of Perovskite $CsPbI_3$ and Its Stabilizing Strategies. *Adv. Funct Materials* **2024**, *34* (14), 2308246.
(23) Wu, W.-Q.; Rudd, P. N.; Ni, Z.; Van Brackle, C. H.; Wei, H.; Wang, Q.; Ecker, B. R.; Gao, Y.; Huang, J. Reducing Surface Halide Deficiency for Efficient and Stable Iodide-Based Perovskite Solar Cells. *J. Am. Chem. Soc.* **2020**, *142* (8), 3989−3996.
(24) Zhang, Z.; Jiang, Z.; Ji, W.; Fu, J.; Wu, T.; Wu, W.; Rui, D.; Xu, P.; Zhou, Y.; Dong, B.; Song, B. Synergistic Defect Passivation by the Treatment of Ionic Liquids for Efficient and Stable Perovskite Solar Cells. *Adv. Energy and Sustain Res.* **2023**, *4* (3), 2200173.
(25) Saidaminov, M. I.; Kim, J.; Jain, A.; Quintero-Bermudez, R.; Tan, H.; Long, G.; Tan, F.; Johnston, A.; Zhao, Y.; Voznyy, O.; Sargent, E. H. Suppression of Atomic Vacancies via Incorporation of Isovalent Small Ions to Increase the Stability of Halide Perovskite Solar Cells in Ambient Air. *Nat. Energy* **2018**, *3* (8), 648−654.
(26) Hassan, A.; Wang, Z.; Ahn, Y. H.; Azam, M.; Khan, A. A.; Farooq, U.; Zubair, M.; Cao, Y. Recent Defect Passivation Drifts and Role of Additive Engineering in Perovskite Photovoltaics. *Nano Energy* **2022**, *101*, 107579.
(27) Song, J.; Xie, H.; Lim, E. L.; Li, Y.; Kong, T.; Zhang, Y.; Zhou, X.; Duan, C.; Bi, D. Multistrategy Toward Highly Efficient and Stable $CsPbI_2Br$ Perovskite Solar Cells Based on Dopant-Free Poly(3-Hexylthiophene). *Solar RRL* **2022**, *6* (4), 2100880.
(28) Zheng, X.; Chen, B.; Dai, J.; Fang, Y.; Bai, Y.; Lin, Y.; Wei, H.; Zeng, X. C.; Huang, J. Defect Passivation in Hybrid Perovskite Solar Cells Using Quaternary Ammonium Halide Anions and Cations. *Nat. Energy* **2017**, *2* (7), 17102.
(29) Xu, J.; Buin, A.; Ip, A. H.; Li, W.; Voznyy, O.; Comin, R.; Yuan, M.; Jeon, S.; Ning, Z.; McDowell, J. J.; Kanjanaboos, P.; Sun, J.-P.; Lan, X.; Quan, L. N.; Kim, D. H.; Hill, I. G.; Maksymovych, P.; Sargent, E. H. Perovskite−Fullerene Hybrid Materials Suppress Hysteresis in Planar Diodes. *Nat. Commun.* **2015**, *6* (1), 7081.
(30) Wu, W.-Q.; Zhong, J.-X.; Liao, J.-F.; Zhang, C.; Zhou, Y.; Feng, W.; Ding, L.; Wang, L.; Kuang, D.-B. Spontaneous Surface/Interface Ligand-Anchored Functionalization for Extremely High Fill Factor over 86% in Perovskite Solar Cells. *Nano Energy* **2020**, *75*, 104929.
(31) Hu, S.; Pascual, J.; Liu, W.; Funasaki, T.; Truong, M. A.; Hira, S.; Hashimoto, R.; Morishita, T.; Nakano, K.; Tajima, K.; Murdey, R.; Nakamura, T.; Wakamiya, A. A Universal Surface Treatment for p−i−n Perovskite Solar Cells. *ACS Appl. Mater. Interfaces* **2022**, *14* (50), 56290−56297.
(32) Chavan, R. D.; Prochowicz, D.; Tavakoli, M. M.; Yadav, P.; Hong, C. K. Surface Treatment of Perovskite Layer with Guanidinium Iodide Leads to Enhanced Moisture Stability and Improved Efficiency of Perovskite Solar Cells. *Adv. Mater. Interfaces* **2020**, *7* (14), 2000105.
(33) Li, F.; Deng, X.; Qi, F.; Li, Z.; Liu, D.; Shen, D.; Qin, M.; Wu, S.; Lin, F.; Jang, S.-H.; Zhang, J.; Lu, X.; Lei, D.; Lee, C.-S.; Zhu, Z.; Jen, A. K.-Y. Regulating Surface Termination for Efficient Inverted Perovskite Solar Cells with Greater Than 23% Efficiency. *J. Am. Chem. Soc.* **2020**, *142* (47), 20134−20142.
(34) Moot, T.; Marshall, A. R.; Wheeler, L. M.; Habisreutinger, S. N.; Schloemer, T. H.; Boyd, C. C.; Dikova, D. R.; Pach, G. F.; Hazarika, A.; McGehee, M. D.; Snaith, H. J.; Luther, J. M. CsI-Antisolvent Adduct Formation in All-Inorganic Metal Halide Perovskites. *Adv. Energy Mater.* **2020**, *10* (9), 1903365.
(35) Sutton, R. J.; Eperon, G. E.; Miranda, L.; Parrott, E. S.; Kamino, B. A.; Patel, J. B.; Hörantner, M. T.; Johnston, M. B.; Haghighirad, A. A.; Moore, D. T.; Snaith, H. J. Bandgap-Tunable Cesium Lead Halide Perovskites with High Thermal Stability for Efficient Solar Cells. *Adv. Energy Mater.* **2016**, *6* (8), 1502458.
(36) Khatibi, A.; Lu, J.; Jensen, J.; Eklund, P.; Hultman, L. Phase Transformations in Face Centered Cubic (Al0.32Cr0.68)2O3 Thin Films. *Surf. Coat. Technol.* **2012**, *206* (14), 3216−3222.
(37) Senkader, S.; Wright, C. D. Models for Phase-Change of Ge2Sb2Te5 in Optical and Electrical Memory Devices. *J. Appl. Phys.* **2004**, *95* (2), 504−511.
(38) Tominaga, J.; Nakano, T.; Atoda, N. Double Optical Phase Transition of GeSbTe Thin Films Sandwiched between Two SiN Layers. *Jpn. J. Appl. Phys.* **1998**, *37* (4R), 1852.
(39) Castaneda, J. F.; Im, J.-H.; Liu, Y.; Liu, S.; Park, N.-G.; Zhang, Y. Domain Size, Temperature, and Time Dependence of Photo-degradation in $MAPbI_3$ Probed by Raman Spectroscopy. *ACS Energy Lett.* **2022**, *7* (9), 3095−3103.

https://doi.org/10.1021/acsenergylett.4c01465
ACS Energy Lett. 2024, 9, 4378−4385

(40) Afify, N. Crystallization Kinetics of Overlapping Phases in Se0.6Ge0.2Sb0.2 Chalcogenide Glass. *J. Non-Cryst. Solids* **1990**, *126* (1−2), 130−140.
(41) Valastro, S.; Mannino, G.; Smecca, E.; Bongiorno, C.; Sanzaro, S.; Deretzis, I.; La Magna, A.; Jena, A. K.; Miyasaka, T.; Alberti, A. Black-Yellow Bandgap Trade-Off During Thermal Stability Tests in Low-Temperature Eu-Doped $CsPbI_3$. *Solar RRL* **2022**, *6* (6), 2200008.
(42) Christian, J. W. *The Theory of Transformations in Metals and Alloys*, 3rd ed.; Pergamon: Oxford Boston, 2002.
(43) Avrami, M. Kinetics of Phase Change. I General Theory. *J. Chem. Phys.* **1939**, *7* (12), 1103−1112.
(44) Avrami, M. Kinetics of Phase Change. II Transformation-Time Relations for Random Distribution of Nuclei. *J. Chem. Phys.* **1940**, *8* (2), 212−224.
(45) Avrami, M. Granulation, Phase Change, and Microstructure Kinetics of Phase Change. III. *J. Chem. Phys.* **1941**, *9* (2), 177−184.
(46) Moghadam, M. M.; Voorhees, P. W. Thin Film Phase Transformation Kinetics: From Theory to Experiment. *Scripta Materialia* **2016**, *124*, 164−168.
(47) Trofimov, V. I.; Trofimov, I. V.; Kim, J.-I. Finite Size Effects in Phase Transformation Kinetics in Thin Films and Surface Layers. *Nuclear Instruments and Methods in Physics Research Section B: Beam Interactions with Materials and Atoms* **2004**, *216*, 334−339.
(48) Pang, E. L.; Vo, N. Q.; Philippe, T.; Voorhees, P. W. Modeling Interface-Controlled Phase Transformation Kinetics in Thin Films. *J. Appl. Phys.* **2015**, *117* (17), 175304.
(49) Fultz, B. *Phase Transitions in Materials*, 1st ed.; Cambridge University Press, 2020. DOI: 10.1017/9781108641449.
(50) Lin, Z.; Zhang, Y.; Gao, M.; Steele, J. A.; Louisia, S.; Yu, S.; Quan, L. N.; Lin, C.-K.; Limmer, D. T.; Yang, P. Kinetics of Moisture-Induced Phase Transformation in Inorganic Halide Perovskite. *Matter* **2021**, *4* (7), 2392−2402.
(51) *CRC Handbook of Chemistry and Physics: A Ready-Reference Book of Chemical and Physical Data, 2016th−2017th*, 97th ed.; Haynes, W. M., Lide, D. R., Bruno, T. J., Eds.; CRC Press: Boca Raton, FL, 2017; pp 771, 775.
(52) Kye, Y.-H.; Yu, C.-J.; Jong, U.-G.; Ri, K.-C.; Kim, J.-S.; Choe, S.-H.; Hong, S.-N.; Li, S.; Wilson, J. N.; Walsh, A. Vacancy-Driven Stabilization of the Cubic Perovskite Polymorph of $CsPbI_3$. *J. Phys. Chem. C* **2019**, *123* (15), 9735−9744.
(53) Boziki, A.; Kubicki, D. J.; Mishra, A.; Meloni, S.; Emsley, L.; Grätzel, M.; Rothlisberger, U. Atomistic Origins of the Limited Phase Stability of Cs^{+}-Rich $FA_x Cs_{(1-x)} PbI_3$ Mixtures. *Chem. Mater.* **2020**, *32* (6), 2605−2614.
(54) Chen, G.-Y.; Guo, Z.-D.; Gong, X.-G.; Yin, W.-J. Kinetic Pathway of γ-to-δ Phase Transition in $CsPbI_3$. *Chem.* **2022**, *8* (11), 3120−3129.
(55) Straus, D. B.; Guo, S.; Cava, R. J. Kinetically Stable Single Crystals of Perovskite-Phase $CsPbI_3$. *J. Am. Chem. Soc.* **2019**, *141* (29), 11435−11439.
(56) Lin, C.-K.; Zhang, Y.; Gao, M.; Lin, J.-A.; Le, H. K. D.; Lin, Z.; Yang, P. Controlling the Phase Transition in $CsPbI_3$ Nanowires. *Nano Lett.* **2022**, *22* (6), 2437−2443.

https://doi.org/10.1021/acsenergylett.4c01465
ACS Energy Lett. 2024, 9, 4378−4385